Electronic Supplementary Information

For the Manuscript Entitled

Polymerization led selective detection and removal of Zn^{2+} and Cd^{2+} ions: Isolation of Zn- and Cd-MOFs and reversibility studies

Saurabh Pandey, Pramod Kumar and Rajeev Gupta*

Department of Chemistry, University of Delhi, Delhi – 110 007

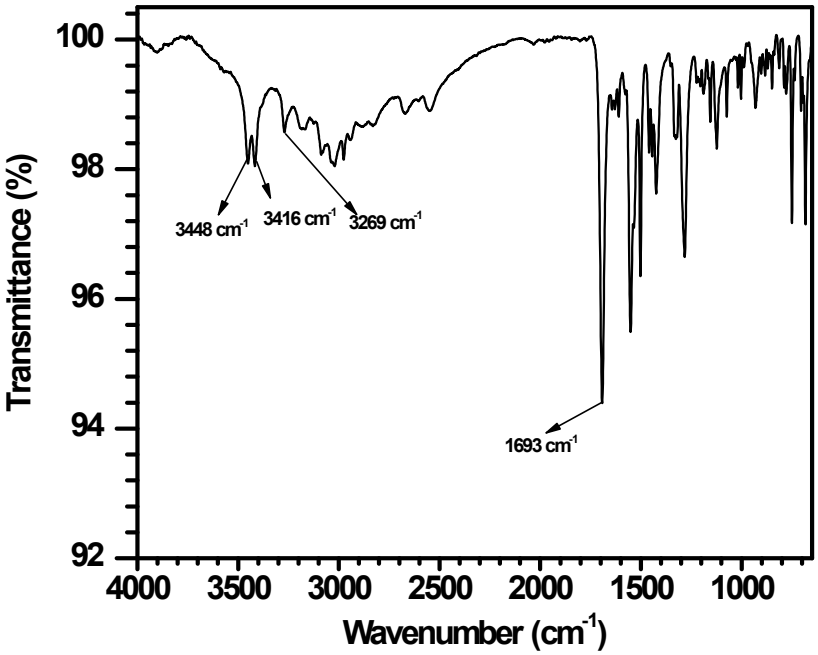

Figure S1. FTIR spectrum of chemosensor **L1**.

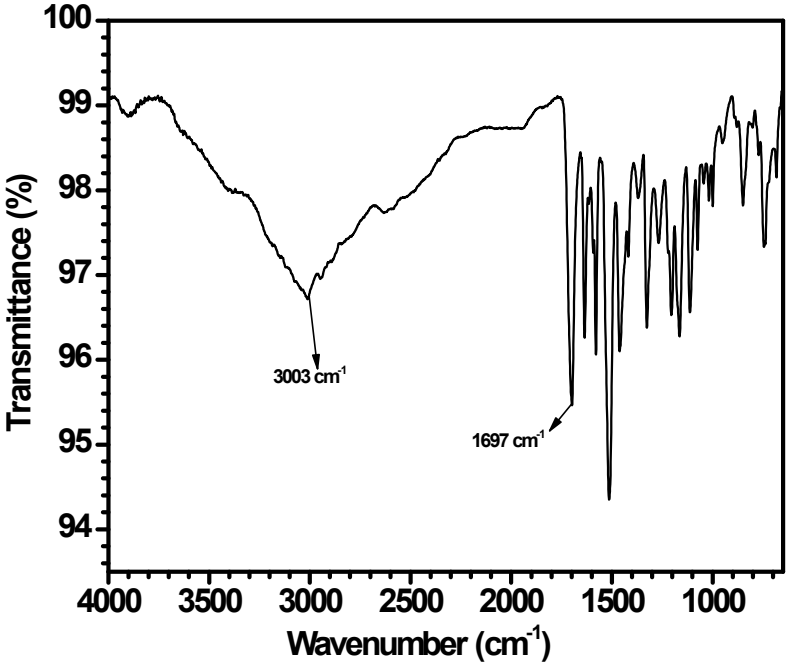

Figure S2. FTIR spectrum of chemosensor **L2**.

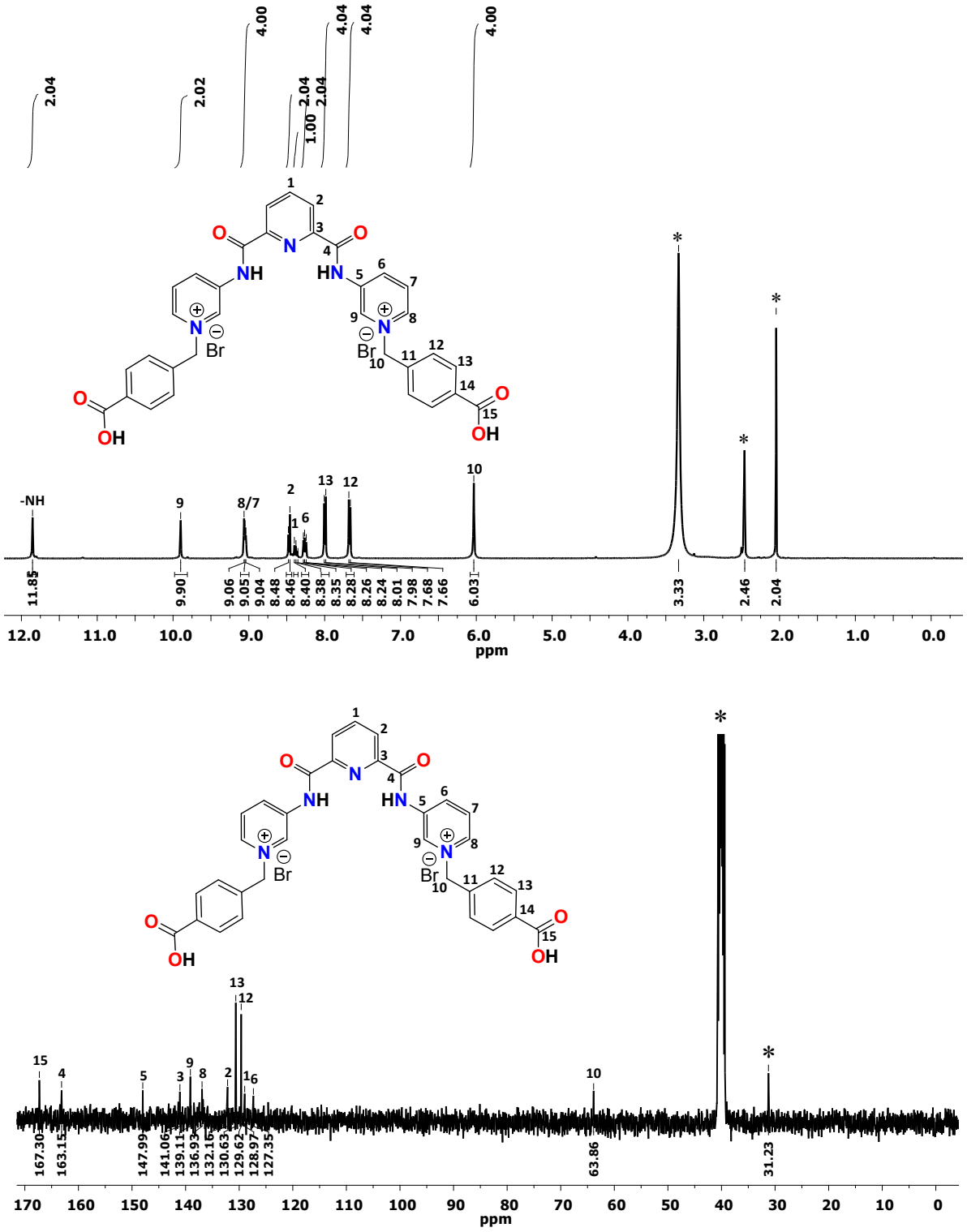

Figure S3. ^{1}H (top) and ^{13}C NMR (bottom) spectra of chemosensor **L1** in DMSO-d_6 where * represents the residual solvent peak(s).

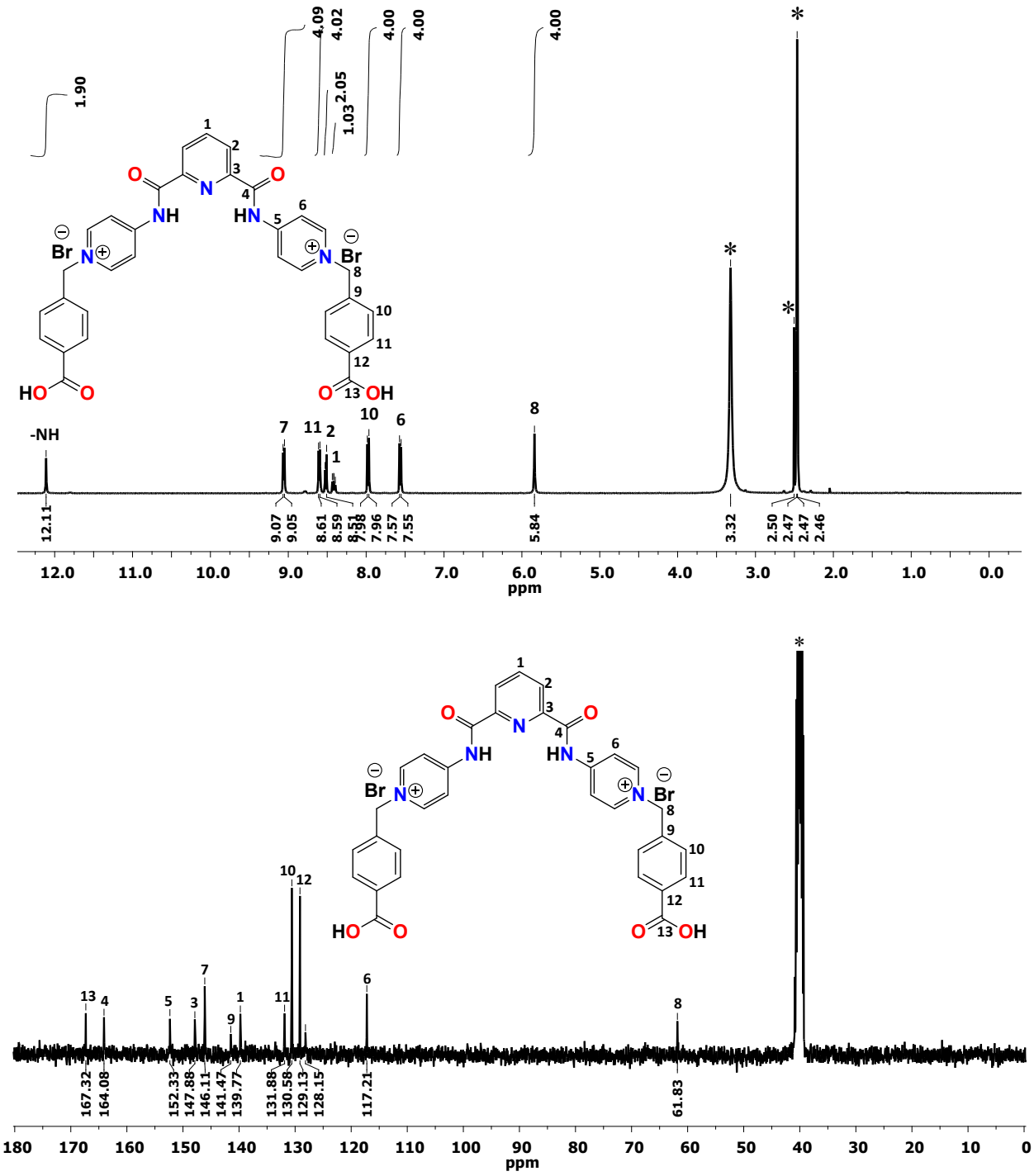

Figure S4. ^{1}H (top) and ^{13}C NMR (bottom) spectra of chemosensor **L2** in DMSO-d_6 where * represents the residual solvent peak(s).

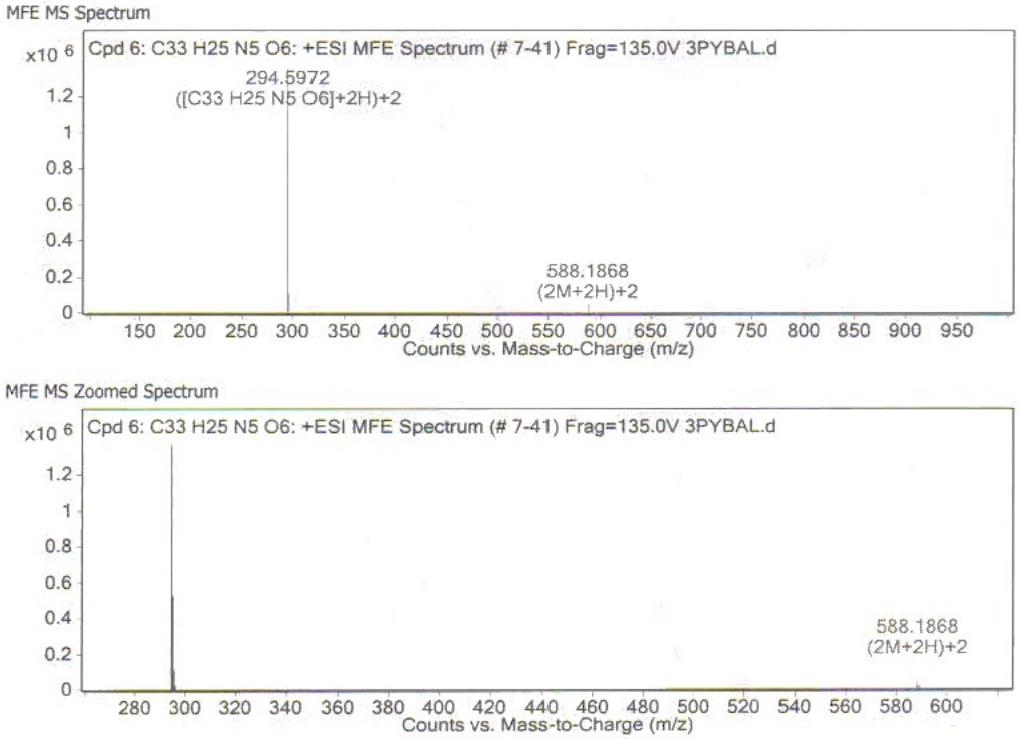

Figure S5. ESI$^+$ mass spectrum of chemosensor **L1** in CH_3OH.

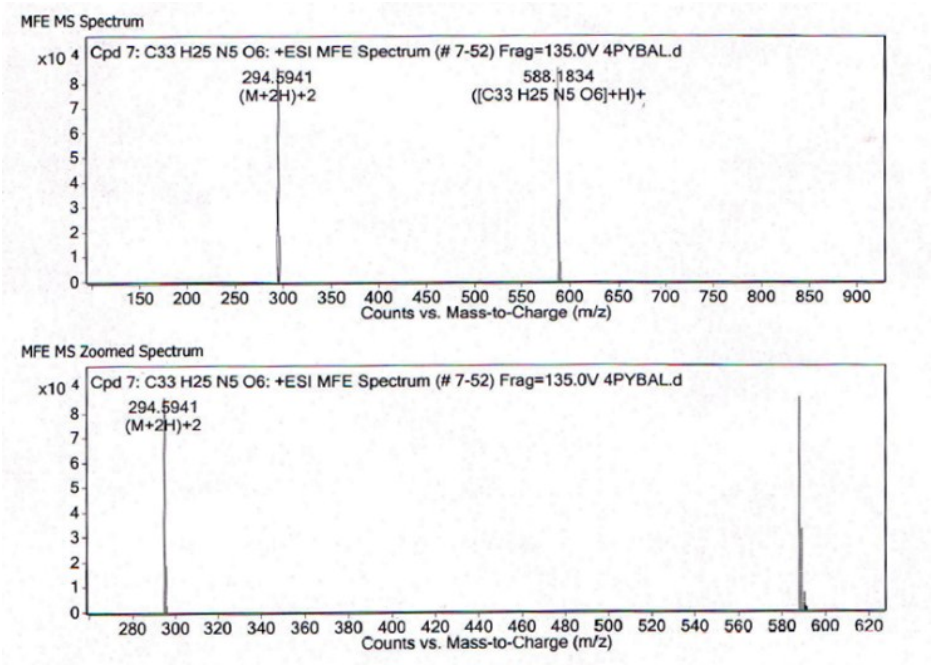

Figure S6. ESI$^+$ mass spectrum of chemosensor **L2** in CH_3OH.

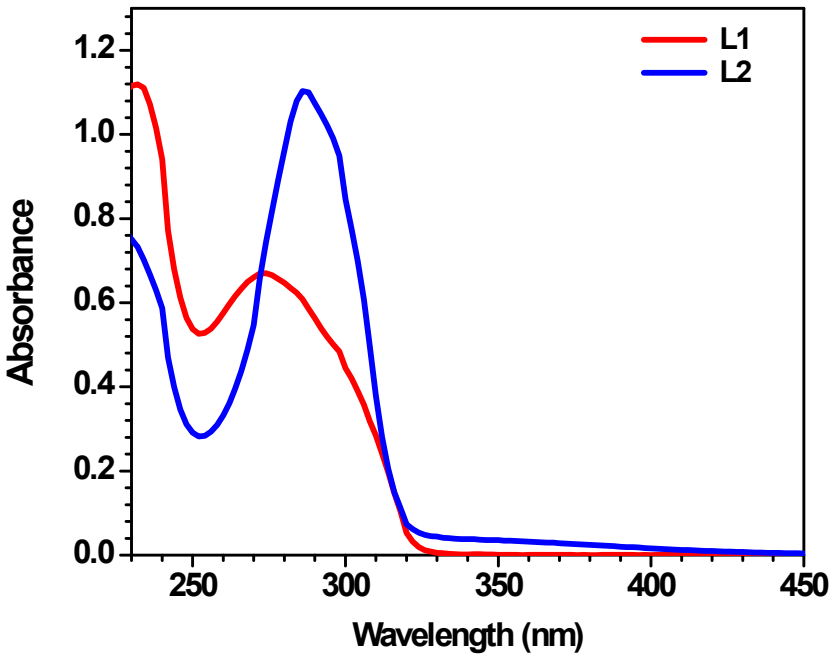

Figure S7. UV-visible spectra of chemosensors **L1** (red trace) and **L2** (blue trace) (20 μM) in CH_3OH.

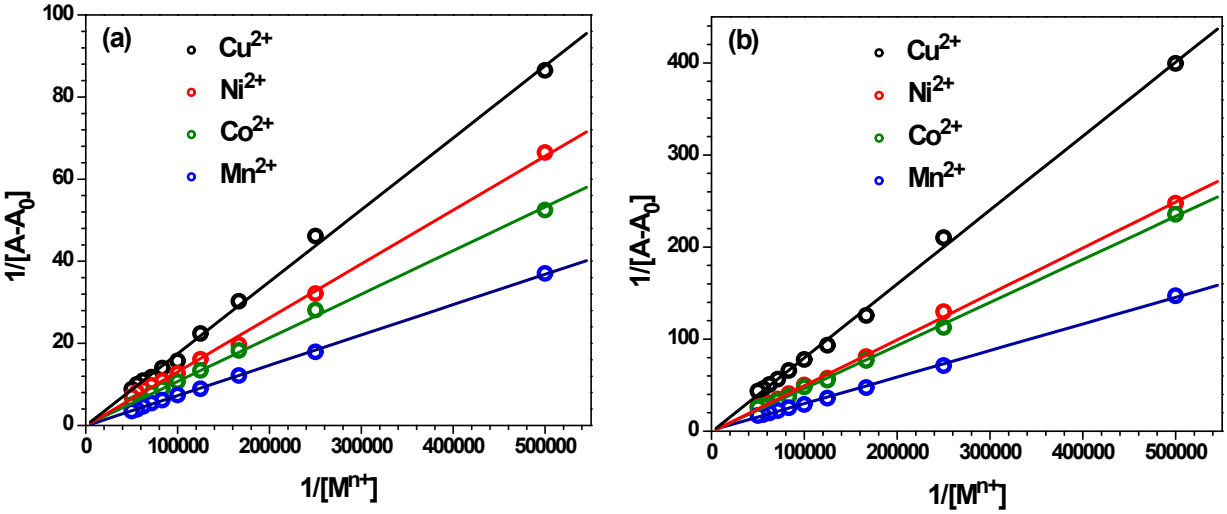

Figure S8. Determination of binding constants for Cu^{2+}, Ni^{2+}, Co^{2+} and Mn^{2+} ions by chemosensors (a) **L1** and (b) **L2** from the UV-visible titrations (at 332 nm) using Benesi-Hildebrand plots in CH_3OH.

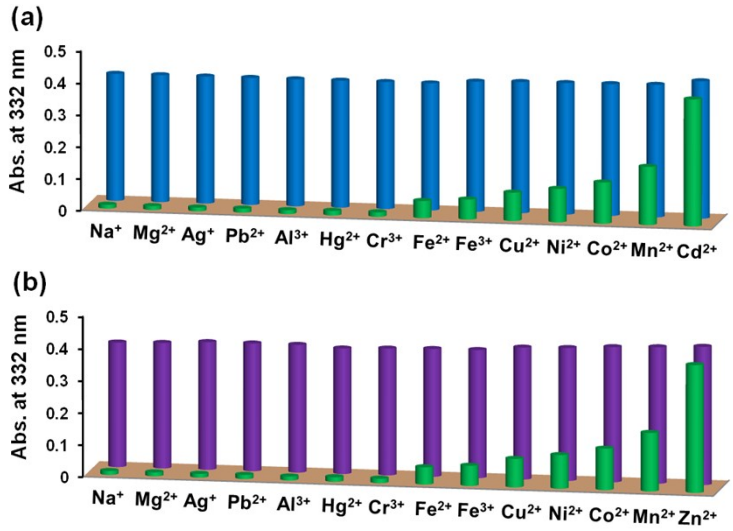

Figure S9. (a) Selectivity of chemosensor **L1** towards Zn^{2+} ion in presence of other metal ions: **L1** + metal ions (green pillars); and **L1** + metal ions + Zn^{2+} ion (blue pillars). (b) Selectivity of chemosensor **L1** towards Cd^{2+} ion in presence of other metal ions: **L1** + metal ions (green pillars); and **L1** + metal ions + Cd^{2+} ion (purple pillars).

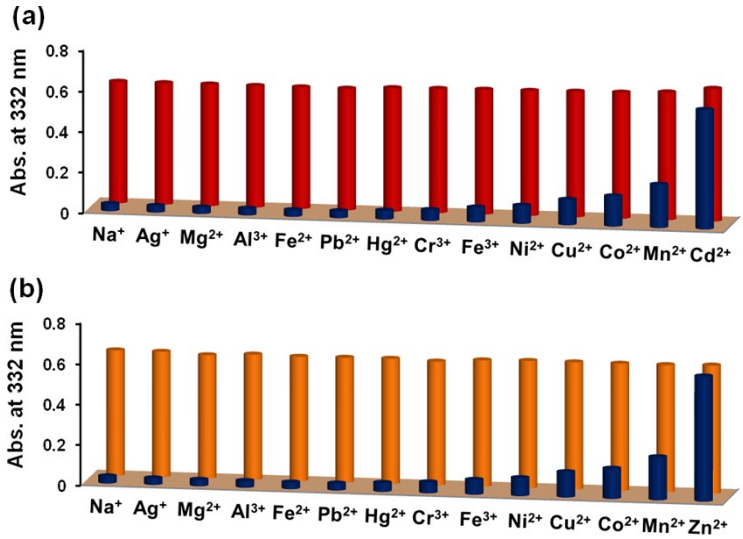

Figure S10. (a) Selectivity of chemosensor **L2** towards Zn^{2+} ion in presence of other metal ions: **L2** + metal ions (blue pillars); and **L2** + metal ions + Zn^{2+} ion (red pillars). (b) Selectivity of chemosensor **L2** towards Cd^{2+} ion in presence of other metal ions: **L2** + metal ions (blue pillars); and **L2** + metal ions + Cd^{2+} ion (yellow pillars).

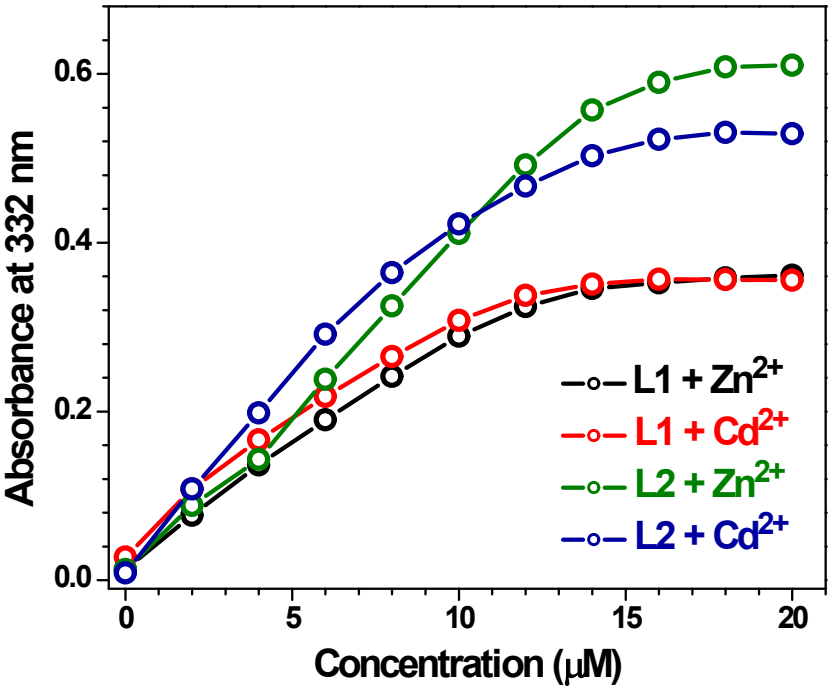

Figure S11. Change in absorbance of chemosensors **L1** (20 μM) and **L2** (20 μM) with 1 equivalent of Zn^{2+}/Cd^{2+} (20 μM) ions in CH_3OH.

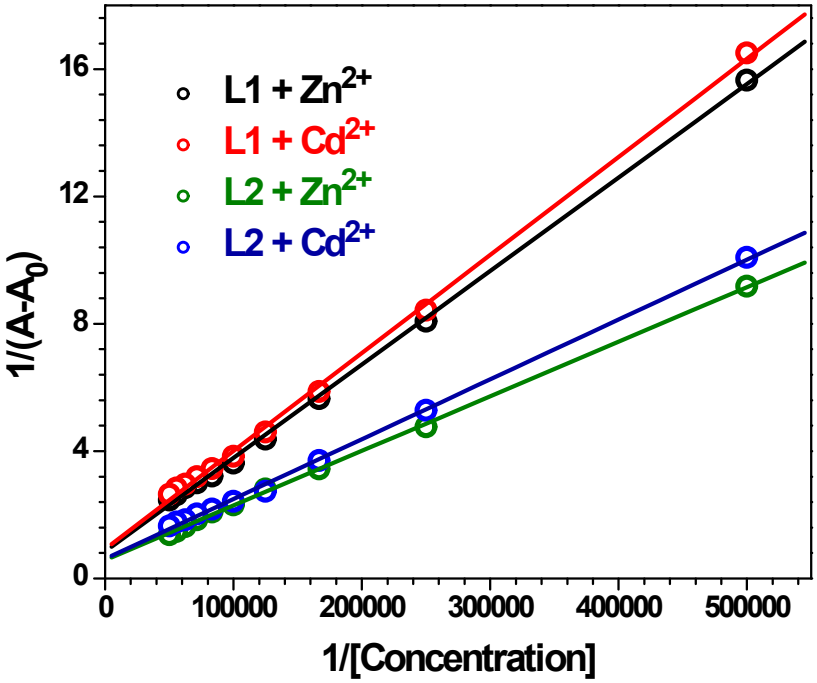

Figure S12. Benesi-Hildebrand plots for the detection of Zn^{2+} and Cd^{2+} ions by chemosensors **L1** and **L2**.

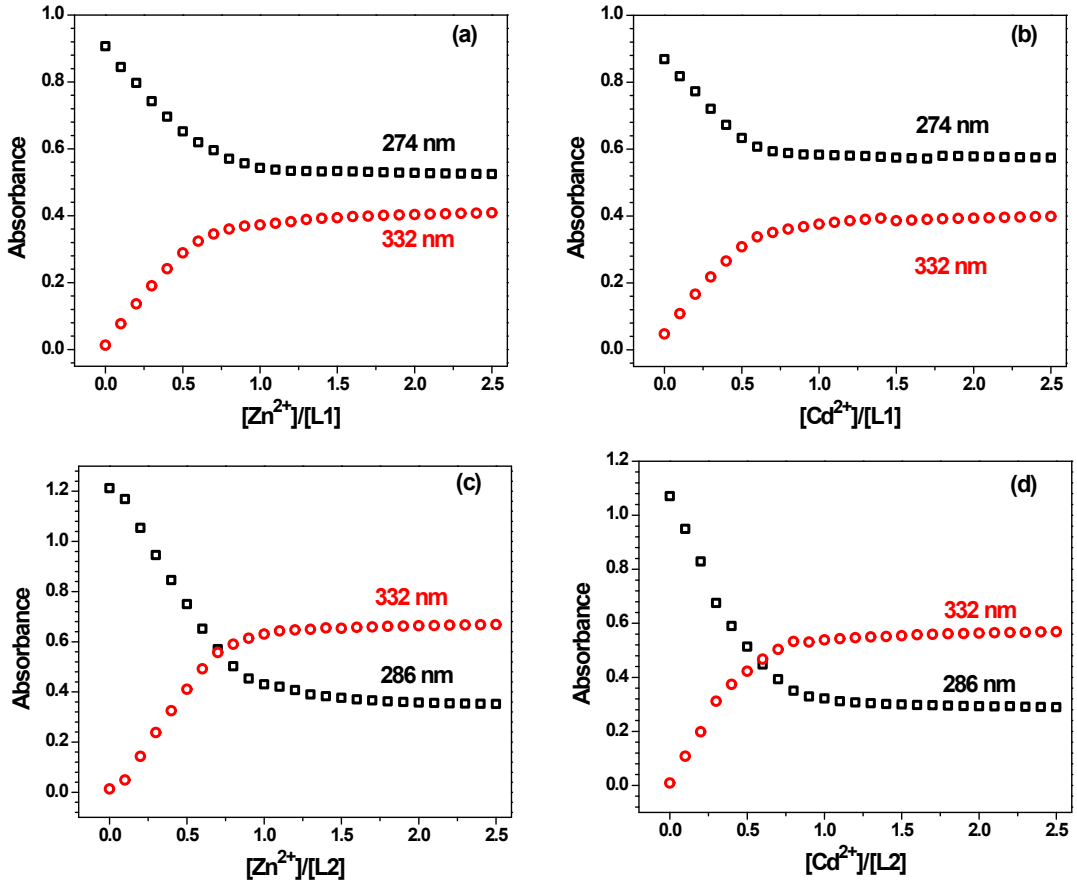

Figure S13. Change in absorbance of chemosensors **L1**/**L2** varied as a function of (a) $[Zn^{2+}]/[\mathbf{L1}]$; (b) $[Cd^{2+}]/[\mathbf{L1}]$; (c) $[Zn^{2+}]/[\mathbf{L2}]$; (d) $[Cd^{2+}]/[\mathbf{L2}]$.

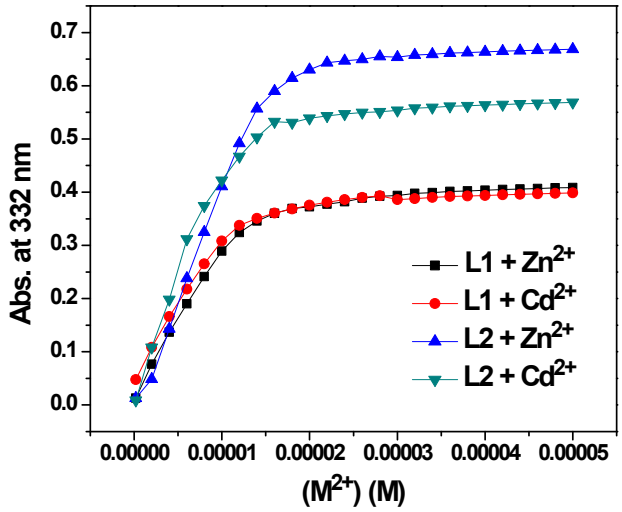

Figure S14. Change in absorbance of chemosensors **L1**/**L2** at 332 nm in methanol with the increase in the concentration of Zn^{2+} or Cd^{2+} ion. $[\mathbf{L1}] = [\mathbf{L2}] = 2.0 \times 10^{-5}$ M.

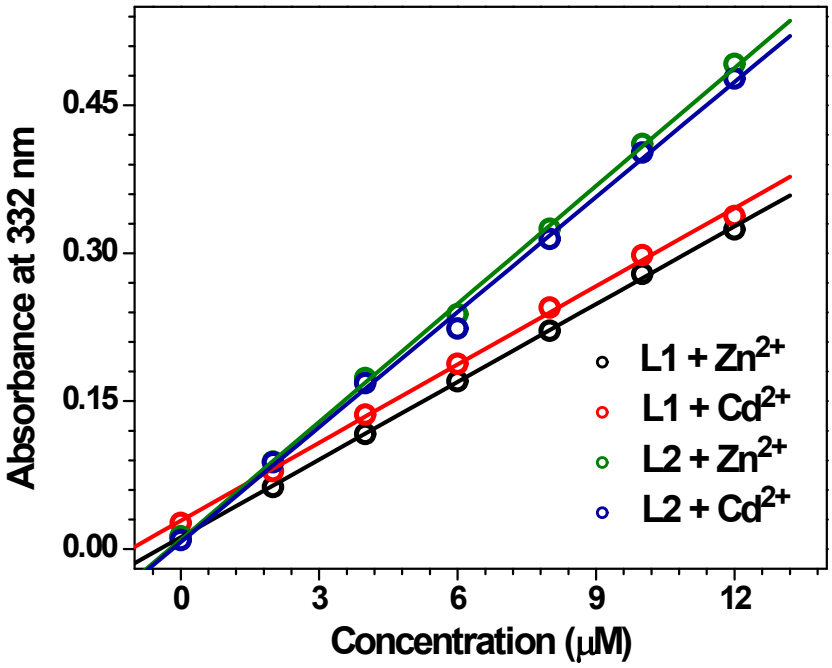

Figure S15. Determination of detection limits by the UV-visible titration for Zn^{2+} and Cd^{2+} ions by using chemosensors **L1** and **L2**.

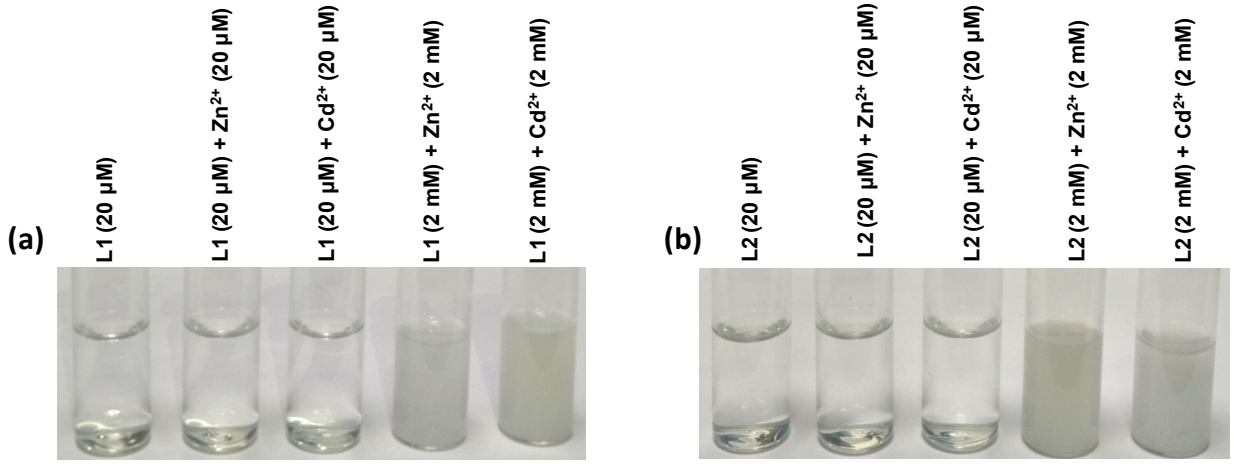

Figure S16. Illustration of effect of concentration on the polymerization-led-precipitation: (a) L1 and (b) L2 in presence of Zn^{2+} and Cd^{2+} ions at 20 μM and 2 mM concentrations.

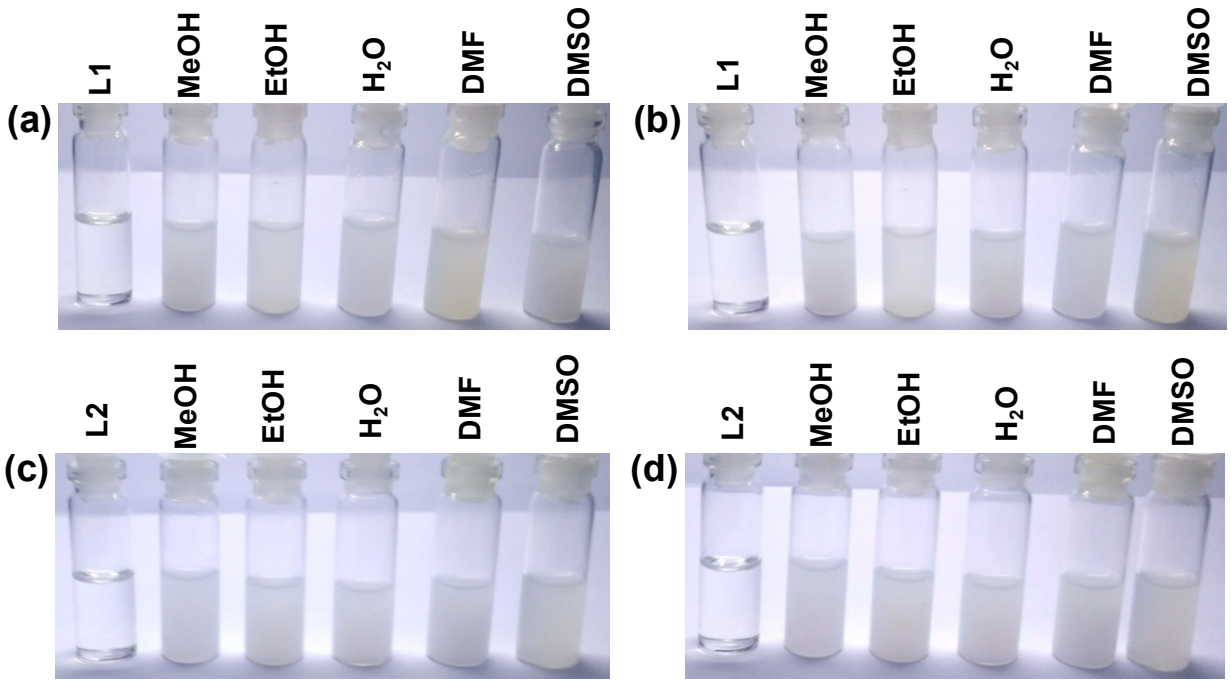

Figure S17. Visible light naked eye detection of (a) Zn^{2+} ion by chemosensor **L1**; (b) Zn^{2+} ion by chemosensor **L2**; (c) Cd^{2+} ion by chemosensor **L1** and (d) Cd^{2+} ion by chemosensor **L2** in different solvent systems via precipitation. Zinc acetate and cadmium acetate were used for all the studies.

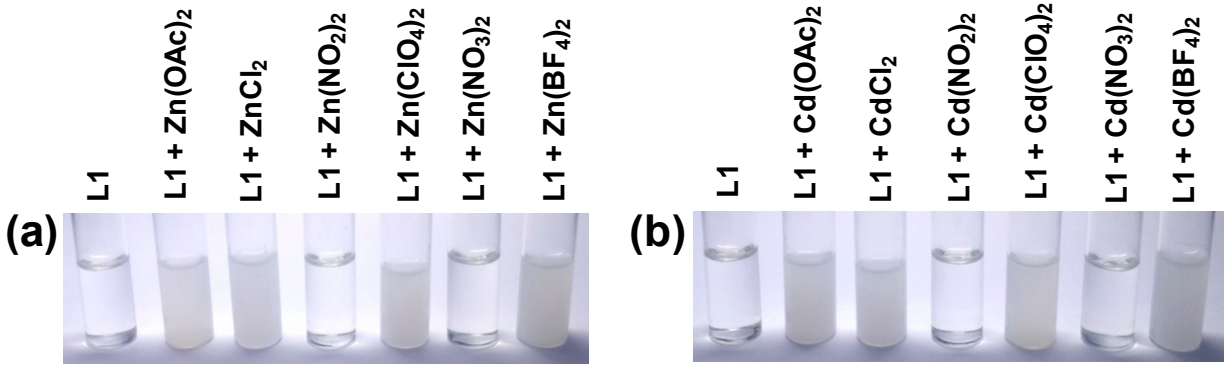

Figure S18. Precipitation induced by different (a) Zn(II) salts; and (b) Cd(II) salts for chemosensor **L1** in methanol.

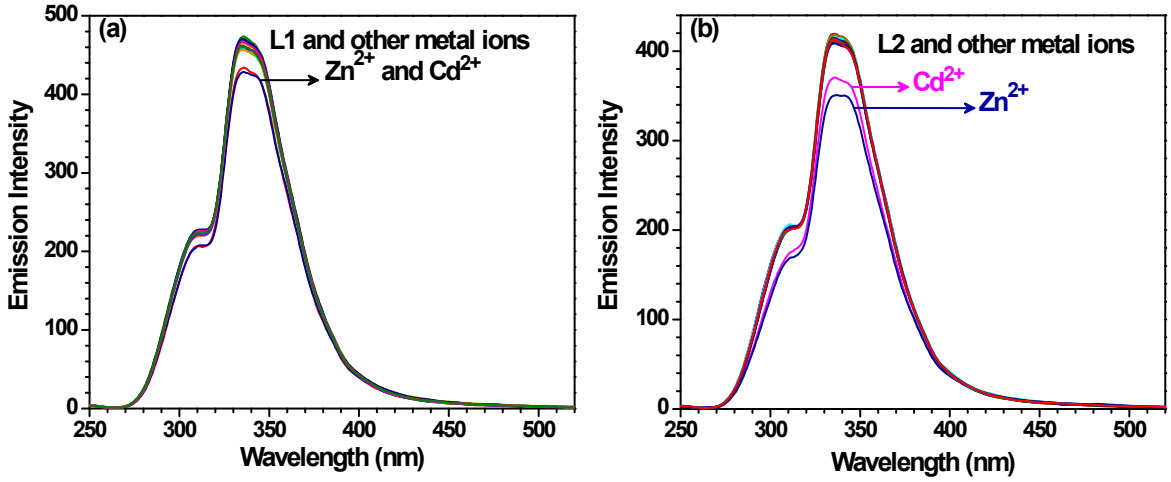

Figure S19. Change in emission of chemosensor (a) **L1** (1μM) (b) **L2** (1 μM) after the addition of 1 equivalent of metal ions (1 μM) in CH_3OH (λ_{ex} = 230 nm).

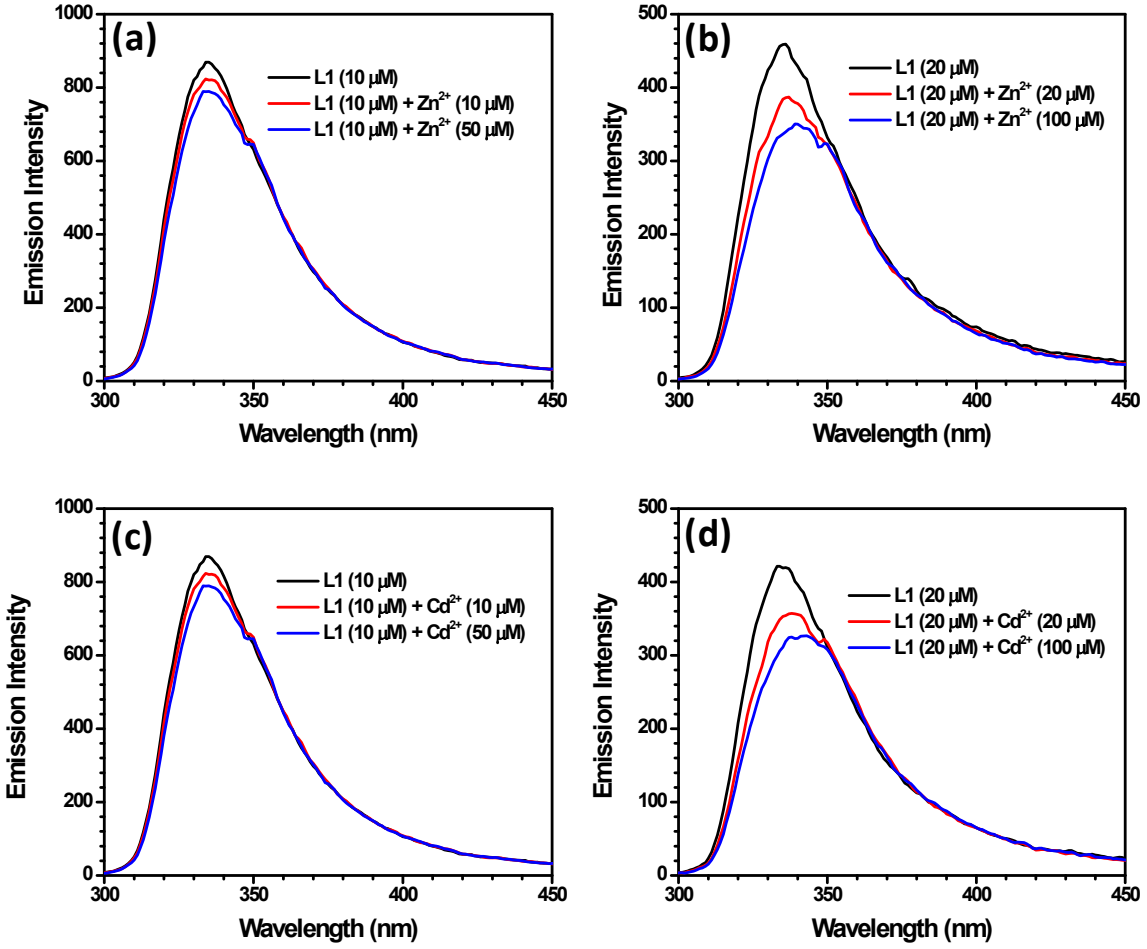

Figure S20. Change in the emission of chemosensor **L1** with different equivalents of Zn^{2+} and Cd^{2+} ions in CH_3OH (λ_{ex} = 230 nm).

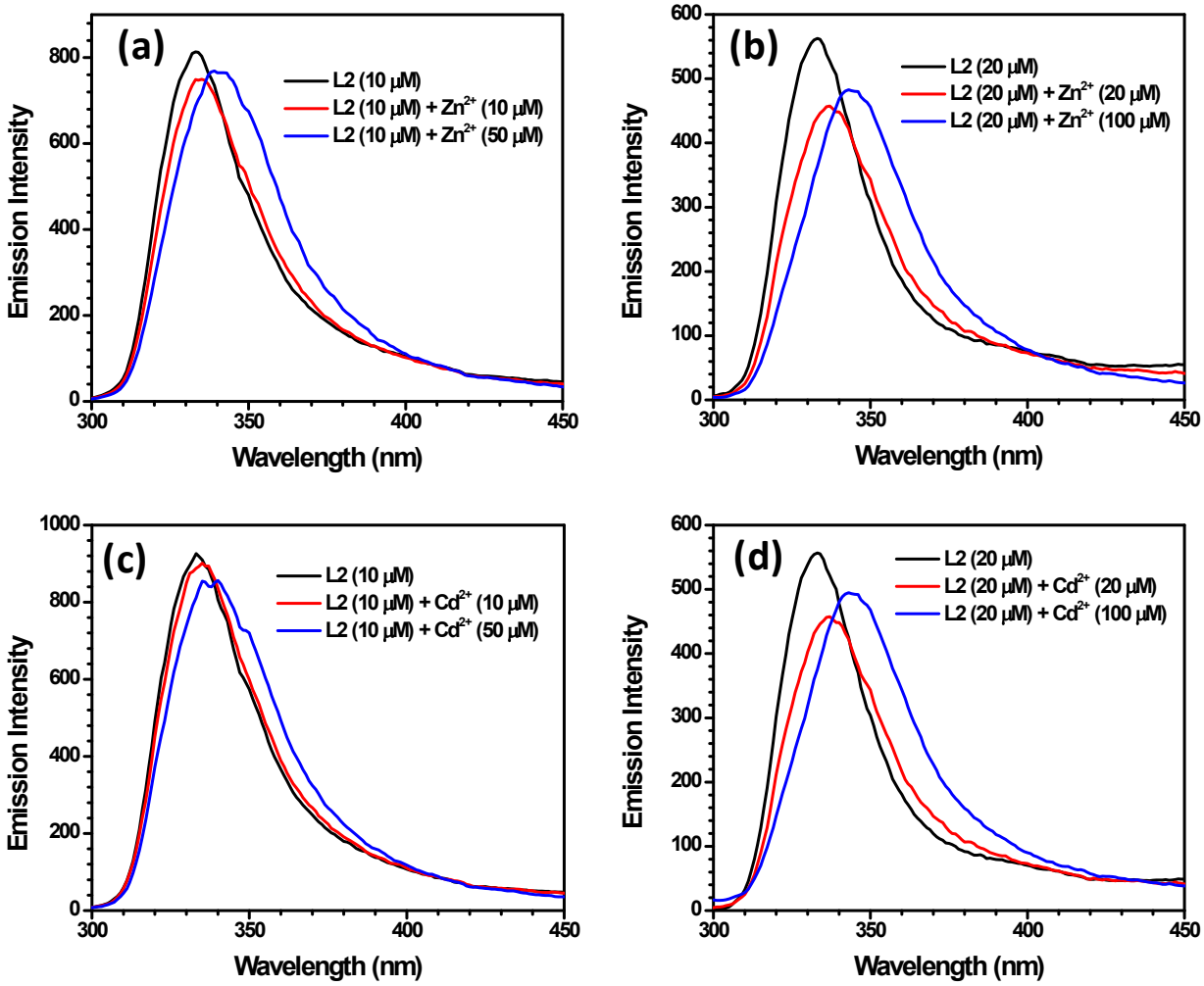

Figure S21. Change in the emission of chemosensor **L2** with different equivalents of Zn^{2+} and Cd^{2+} ions in CH_3OH (λ_{ex} = 230 nm).

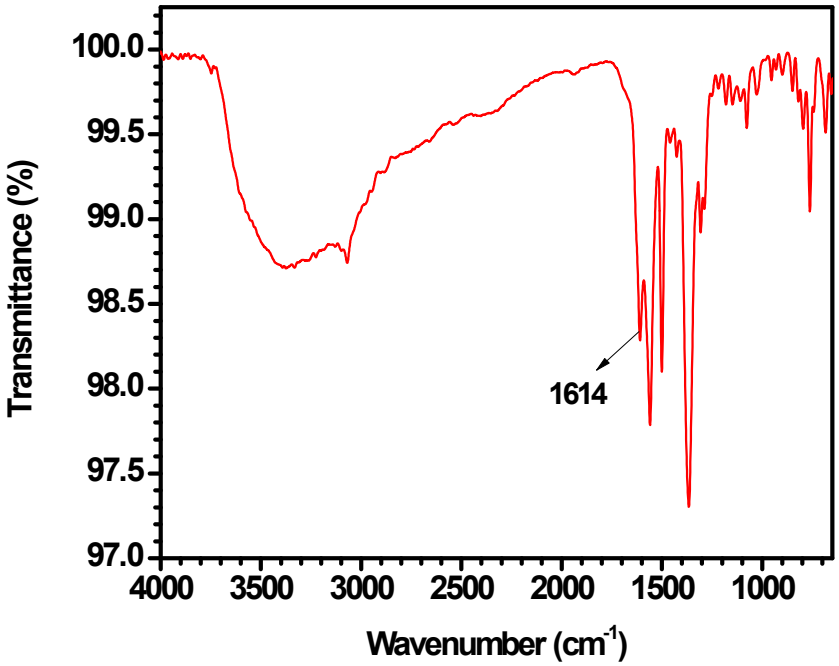

Figure S22. FTIR spectrum of Zn(II)-**L1**.

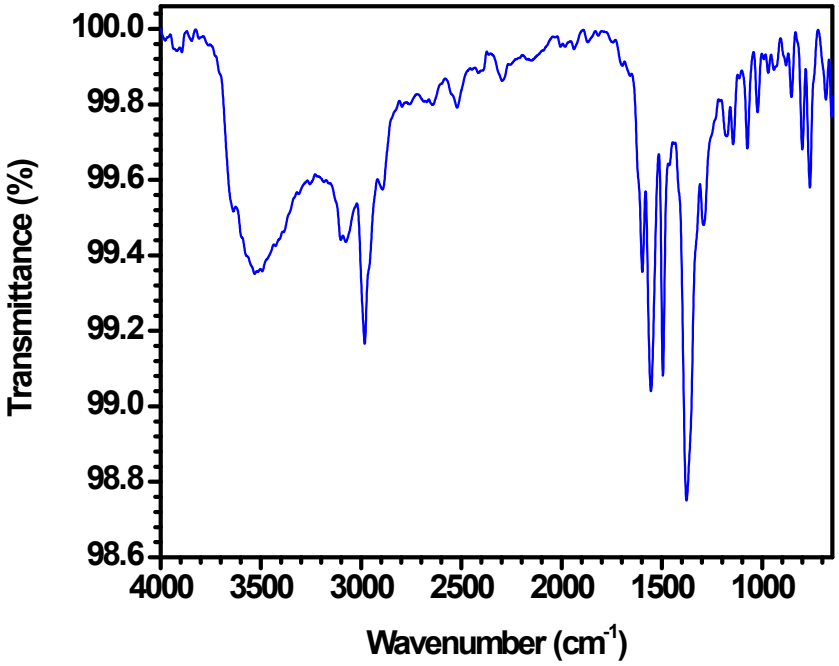

Figure S23. FTIR spectrum of Cd(II)-**L1**.

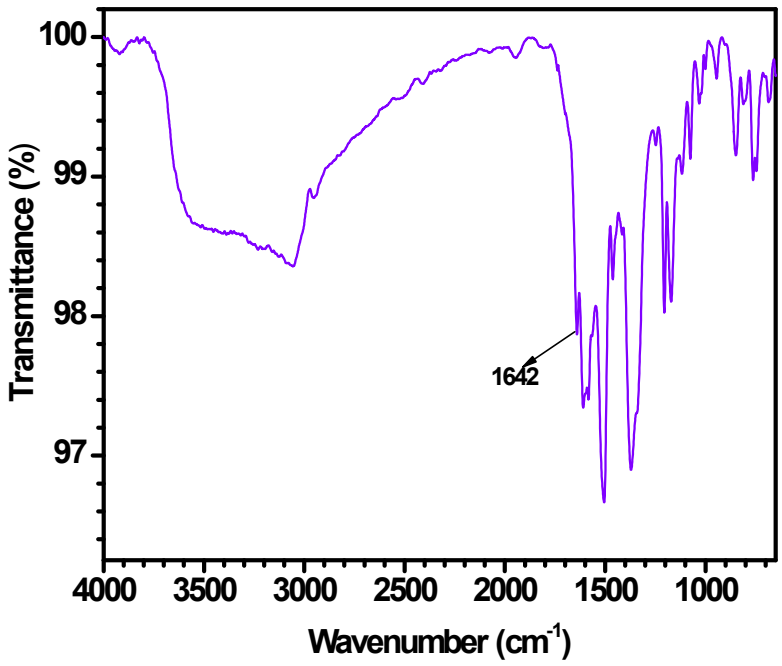

Figure S24. FTIR spectrum of Zn(II)-**L2**.

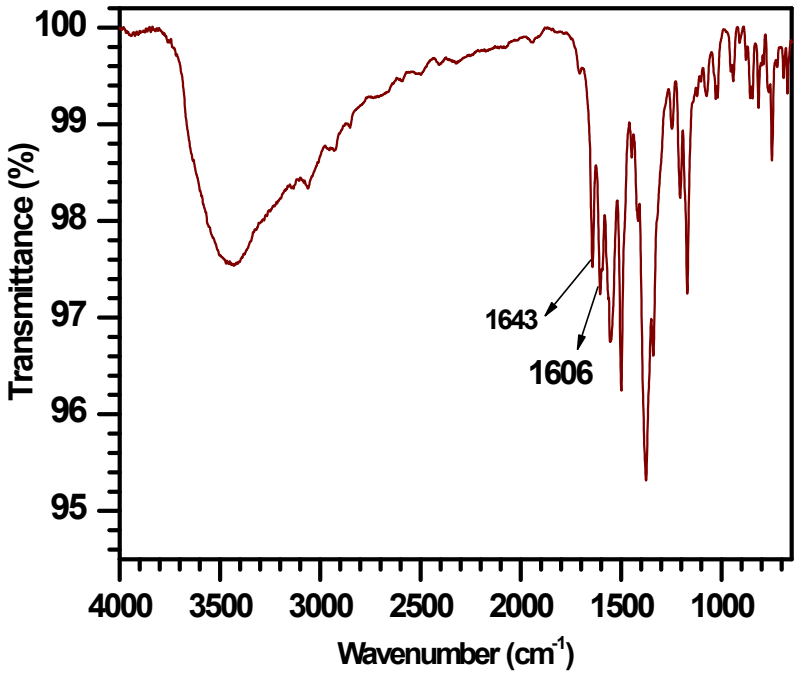

Figure S25. FTIR spectrum of Cd(II)-**L2**.

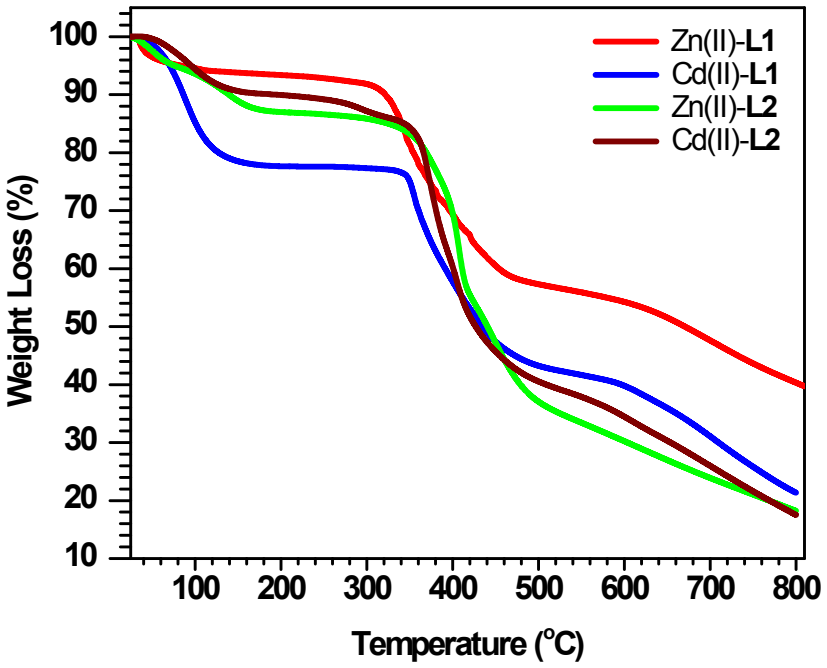

Figure S26. Thermal Gravimetric Analysis (TGA) plots for Zn(II)-**L1** (red trace), Cd(II)-**L1** (blue trace), Zn(II)-**L2** (green trace) and Cd(II)-**L2** (wine trace).

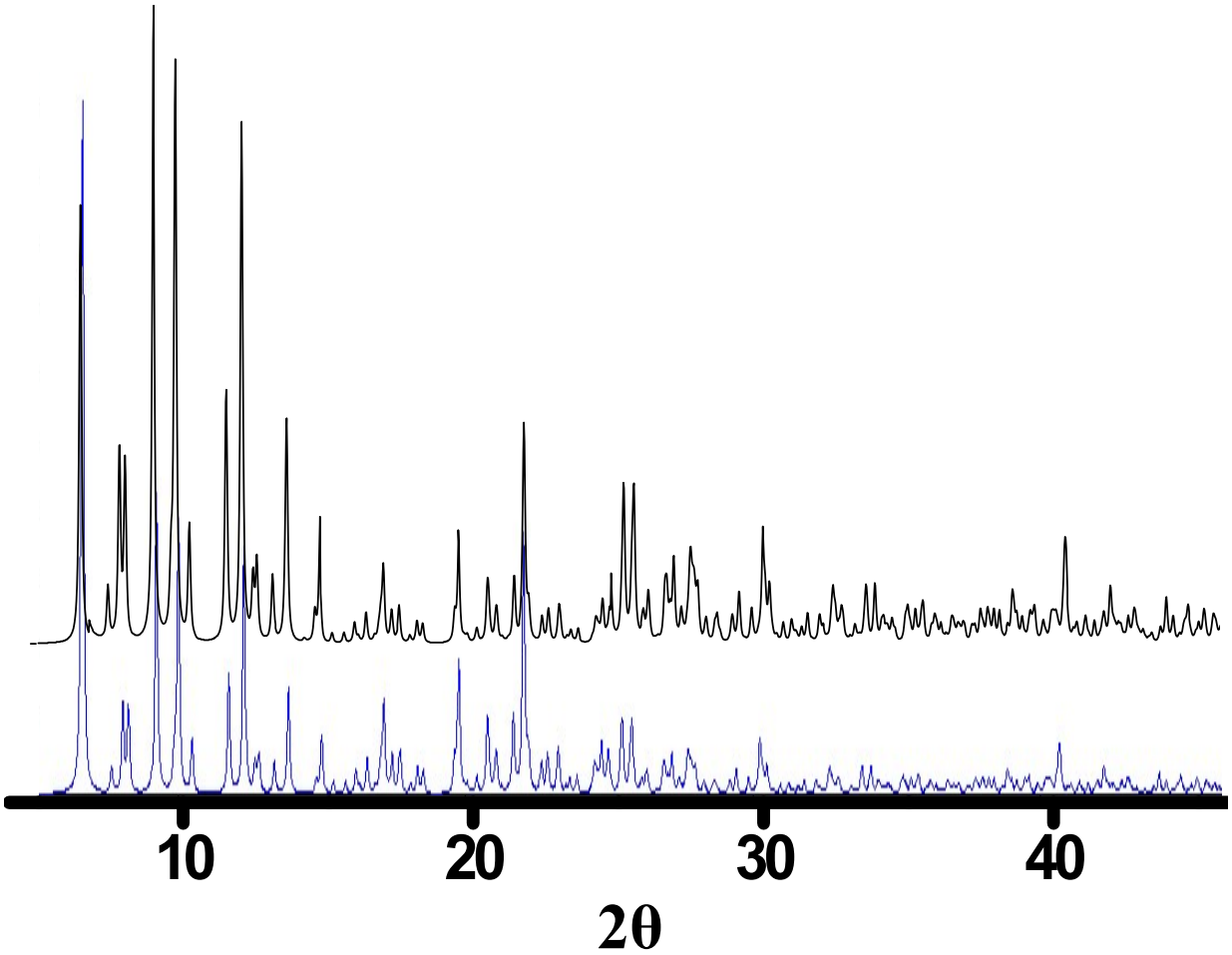

Figure S27. X-ray powder diffraction patterns for as-synthesized **Cd(II)-L1** (black trace) and the one simulated from Mercury 3.0 using single crystal diffraction data (blue trace) of **Cd(II)-L1**.

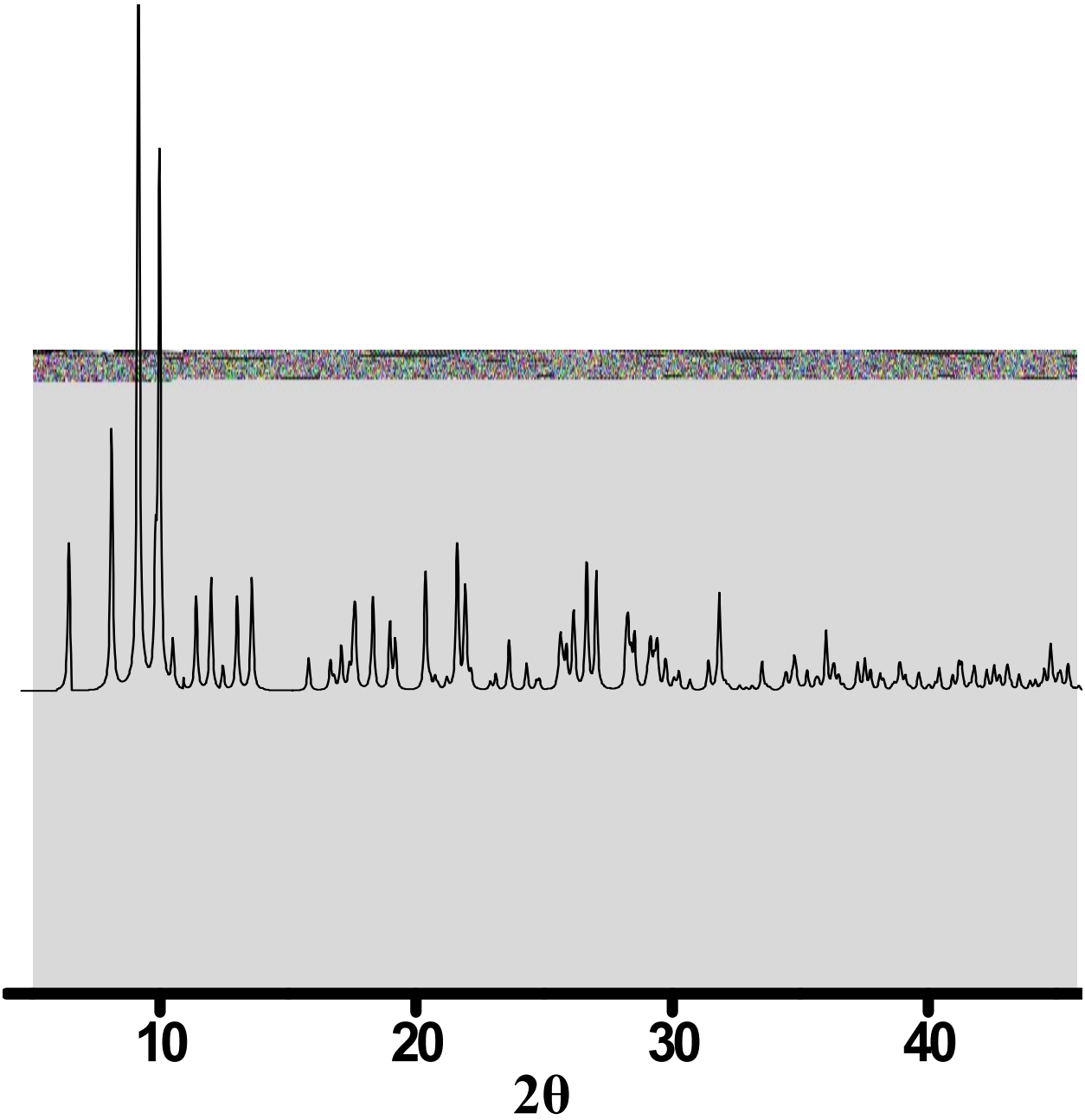

Figure S28. X-ray powder diffraction patterns for as-synthesized **Zn(II)-L1** (black trace) and the one simulated from Mercury 3.0 using single crystal diffraction data (blue trace) of **Cd(II)-L1**.

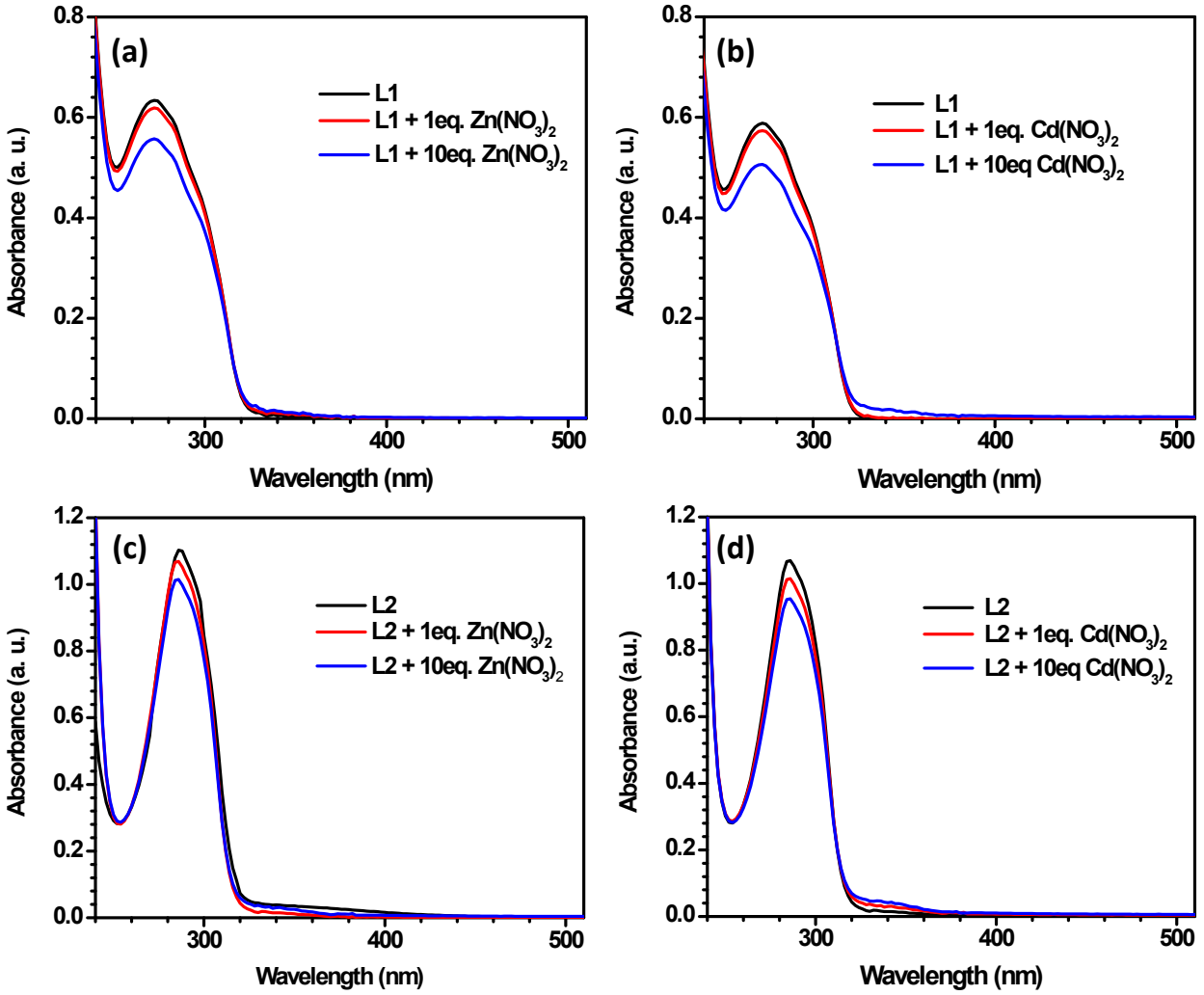

Figure S29. Change in absorbance of chemosensor (a) **L1** (20 μM) with 1 equivalent of $Zn(NO_3)_2$ (20 μM) ion (b) **L1** (20 μM) with 1 equivalent of $Cd(NO_3)_2$ (20 μM) ion (c) **L2** (20 μM) with 1 equivalent of $Zn(NO_3)_2$ (20 μM) ion (d) **L2** (20 μM) with 1 equivalent of $Cd(NO_3)_2$ (20 μM) ion in CH_3OH.

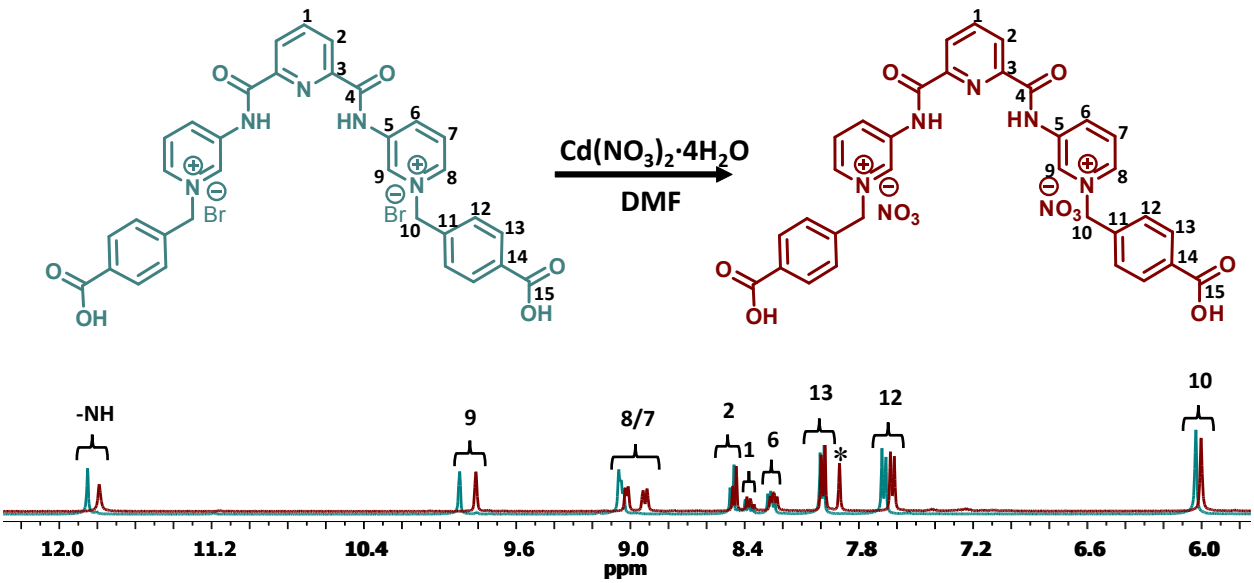

Figure S30. Partial ^{1}H NMR spectra of chemosensor **L1** (dark cyan trace) and after the addition of $Cd(NO_3)_2$ (wine trace) recorded in DMSO-d_6 solvent. * represents the C(O)–H proton of DMF molecule.

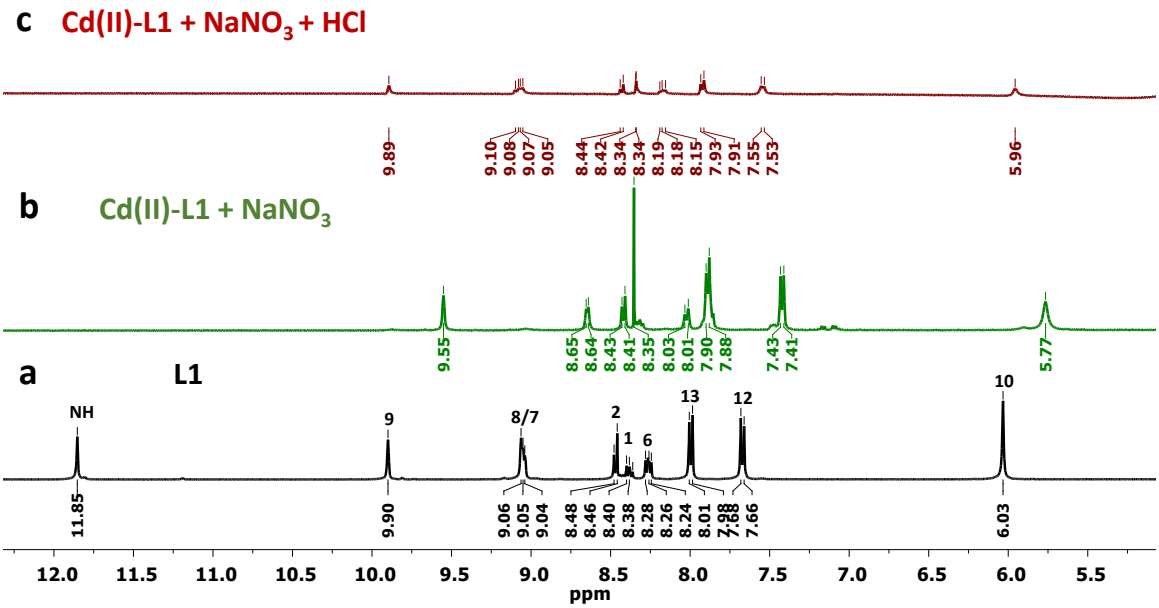

Figure S31. ^{1}H NMR spectrum of (a) **L1** (black trace); (b) Cd(II)-**L1** after the addition of $NaNO_3$ (green trace); and (c) after further addition of HCl (wine trace).

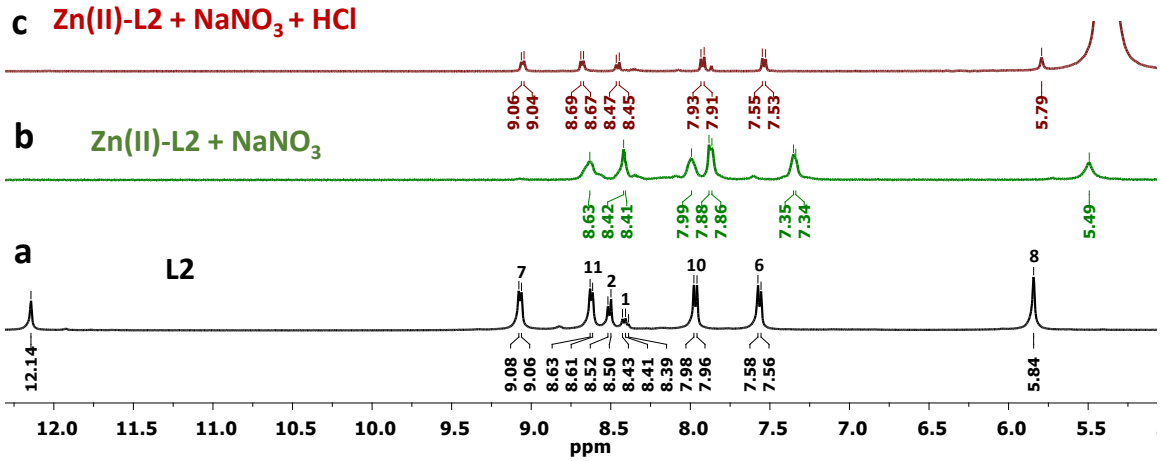

Figure S32. ^{1}H NMR spectrum of (a) **L2** (black trace); (b) Zn(II)-**L2** after the addition of $NaNO_3$ (green trace); and after (c) further addition of HCl (wine trace).

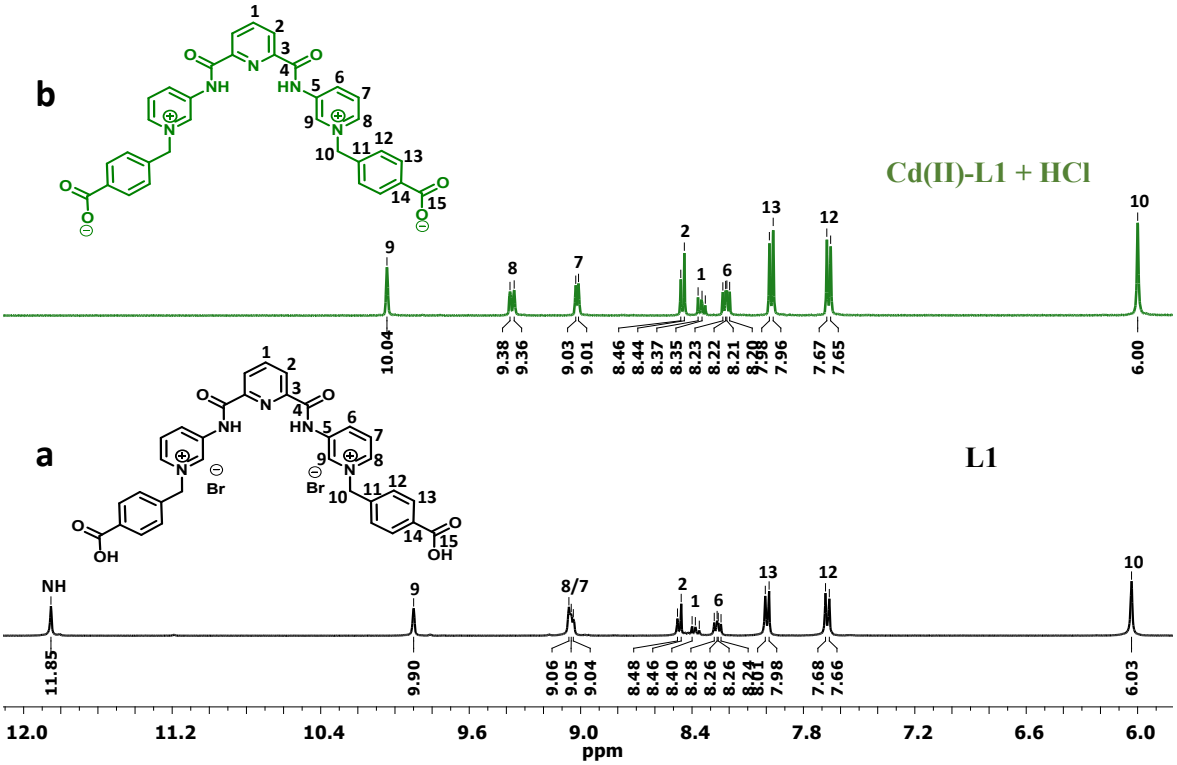

Figure S33. ^{1}H NMR spectrum of **L1** (black trace) and Cd(II)-**L1** (green trace) after the addition of HCl maintaining pH = 6 (green trace).

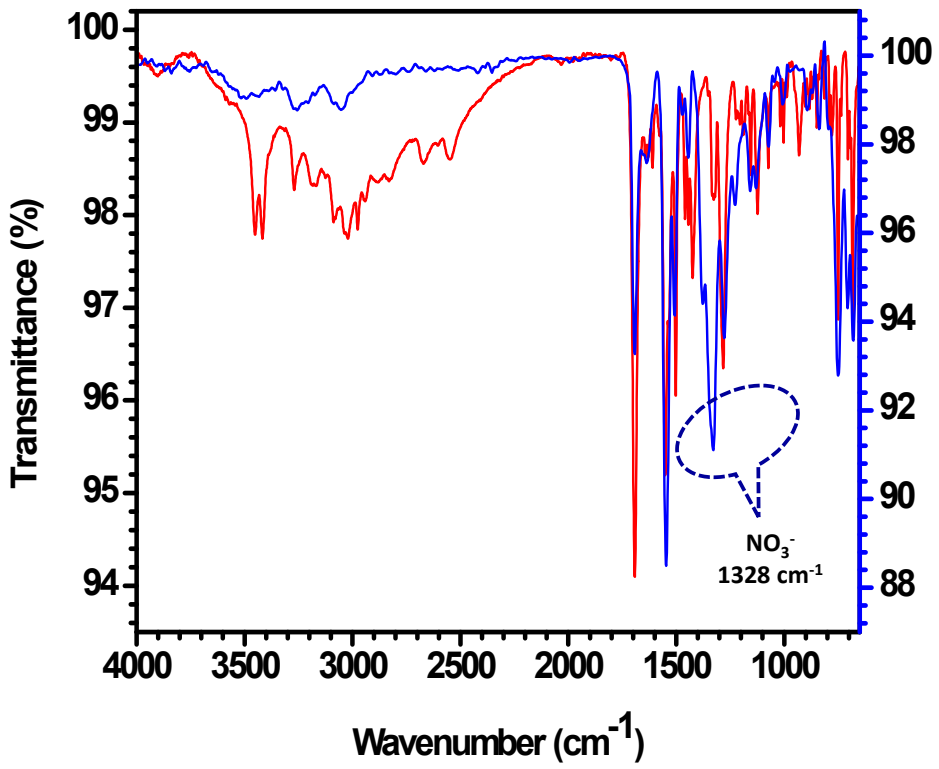

Figure S34. FTIR spectra of **L1** (red trace) and **L1–NO_3** adduct (blue trace).

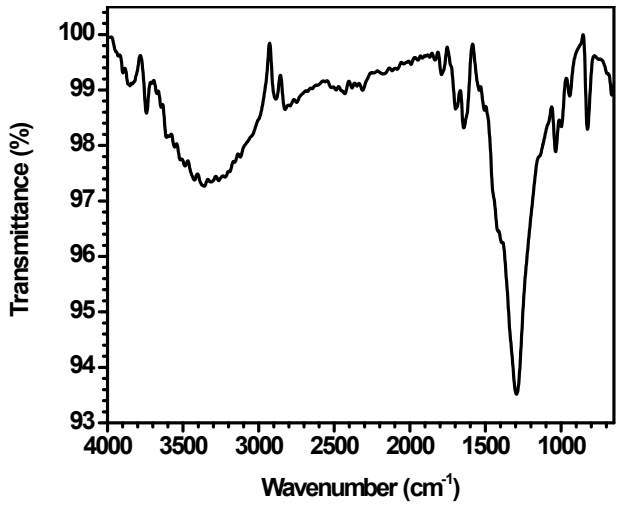

Figure S35. FTIR spectrum of isolated cadmium nitrate salt from a reaction of **Cd-MOF** with $NaNO_3$ in DMSO.

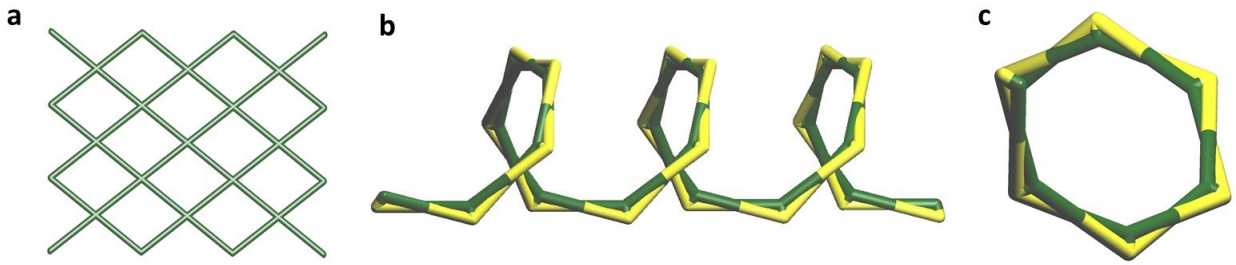

Figure S36. Topological representation of (a) Cd(II)-**L1**-A and Cd(II)-**L1**-B along (b) *a*- and (c) *c*-axis, respectively. Color code: yellow, Cd; green, contribution from L1.

Table S1. Binding constants (K_b) for Cu^{2+}, Ni^{2+}, Co^{2+} and Mn^{2+} ions by chemosensors **L1** and **L2** from UV-visible titrations (at 332 nm) using Benesi-Hildebrand plots in CH_3OH.

Species	**Kb (M^{-1})**	**Species**	**Kb (M^{-1})**
L1 + Cu^{2+}	1.24×10^2	**L2 + Cu^{2+}**	8.37×10^2
L1 + Ni^{2+}	6.38×10^2	**L2 + Ni^{2+}**	1.01×10^3
L1 + Co^{2+}	7.99×10^2	**L2 + Co^{2+}**	1.06×10^3
L1 + Mn^{2+}	1.56×10^3	**L2 + Mn^{2+}**	3.58×10^3
L1 + Zn^{2+}	2.90×10^4	**L2 + Zn^{2+}**	3.38×10^4
L1 + Cd^{2+}	2.99×10^4	**L2 + Cd^{2+}**	3.28×10^4

Table S2. Crystallographic data collection and structure refinement parameters for Cd(II)-**L1-B**, Zn(II)-**L2** and Cd(II)-**L2**.

Complex	Cd(II)-**L1-B**	Zn(II)-**L2**	Cd(II)-**L2**
CCDC No.	**1863806**	**1828072**	**1828071**
Formula	C99 H109 Cd3 N15 O38	C33 H47 Zn N5 O18	C33 H47 Cd N5 O18
Fw	2454.22	867.13	914.15
T(K)	100(2) K	273(2) K	100(2) K
Crystal System	orthorhombic	monoclinic	monoclinic
Space Group	$P2_12_12_1$	*I2/c*	*C2/c*
a(Å)	14.3557(9)	18.5144(18)	22.987(7)
b(Å)	24.1536(15)	13.2579(13)	12.635(3)
c(Å)	33.691(2)	18.8316(18)	19.051(5)
α(°)	90°	90°	90°
β(°)	90°	105.277(9)°	124.699(11)°
γ(°)	90°	90°	90°
V(Å^3)	11682.1(3)	4459.1(8)	4549(2)
Z	4	4	4
d(Mg/m^3)	1.395	1.292	1.335
F(000)	4826	1336	1408
Goodness-of-fit on F^2	1.084	1.041	1.113
R_1,wR_2 [I>2(I)]	0.0548, 0.1439	0.1077, 0.2820	0.1031, 0.2545
R_1,wR_2[all data]	0.0648, 0.1554	0.1808, 0.3225	0.1142, 0.2608

$^aR_1 = \sum \quad ||F_o| - |F_c|| / \sum |F_o|$; $wR_2 = \{\sum [w(/|F_o|^2 - |F_c|^2)^2] / \sum[w F_o^4]\}^{1/2}$

Table S3. Selected bond distances and angles for Cd(II)-**L1-B**, Zn(II)-**L2** and Cd(II)-**L2**.

Bond Length (Å)			
Bond	Cd(II)-**L1-B**	Zn(II)-**L2**	Cd(II)-**L2**
N(1)-M(1)	2.350(6)	2.226(7)	2.373(8)
N(2)-M(1)	2.296(6)	1.967(14)	2.258(10)
N(3)-M(1)	2.366(7)		
O(2)-M(1)			2.584(7)
O(3)-M(1)	2.462(5)	1.990(5)	2.277(6)
O(4)-M(1)	2.313(5)		
O(5)-M(1)	2.295(7)		
O(6)-M(1)	2.714(1)		
Bond Angle (Å)			
	Cd(II)-**L1-B**	Zn(II)-**L2**	Cd(II)-**L2**
N(2)-M(1)-N(1)	70.1(2)	76.8(2)	70.65(19)
N(2)- M(1) O(3)	93.27(19)	130.54(18)	137.75(18)
N(2)- M(1) O(2)			84.99(17)
N(1)- M(1) O(2)			88.7(2)
O(3)- M(1)-N(1)	96.1(2)	99.7(2)	102.9(3)
N(2)- M(1)-N(3)	70.4(2)		
O(3)- M(1)-N(3)	84.6(2)		
N(3)- M(1)-N(1)	140.5(2)		
N(2)- M(1)-O(5)	99.9(3)		
O(3)- M(1)-O(5)	166.8(3)		
N(3)- M(1)-O(5)	100.4(2)		
O(5)- M(1)-N(1)	87.7(3)		
N(2)- M(1)-O(6)	142.0(3)		
O(3)- M(1)-O(4)	54.48(17)		
N(3)- M(1)-O(6)	90.1(3)		
O(4)- M(1)-O(5)	112.7(2)		
N(1)- M(1)-O(6)	122.9(3)		

Where M(1) = Zn^{2+} [for Zn(II)-**L2**] and Cd^{2+} [for Cd(II)-**L1-**B and Cd(II)-**L2**].